Encapsulated Inorganic Nanostructures: A Route to Sizable Modulated, Noncovalent, On-Tube Potentials in Carbon Nanotubes

Adelina Ilie,[†,*] James S. Bendall,[‡] Katsumi Nagaoka,[§] Stefan Egger,[⊥] Tomonobu Nakayama,[§] and Simon Crampin[†]

[†]Department of Physics, University of Bath, Bath BA2 7AY, United Kingdom, [‡]Nanoscience, University of Cambridge, 11 J.J. Thomson Avenue, Cambridge CB3 0FF, United Kingdom, [§]Nano System Functionality Centre, MANA, National Institute for Materials Science, 1-1, Namiki, Tsukuba, Ibaraki 305-0044, Japan, and [⊥]Empa. Swiss Federal Laboratories for Materials Science and Technology, Uberlandstrasse 129, CH-8600 Dübendorf, Switzerland

ABSTRACT The large variety of hybrid carbon nanotube systems synthesized to date (*e.g.*, by encapsulation, wrapping, or stacking) has provided a body of interactions with which to modify the host nanotubes to produce new functionalities and control their behavior. Each, however, has limitations: hybridization can strongly degrade desirable nanotube properties; noncovalent interactions with molecular systems are generally weak; and interlayer interactions in layered nanotubes are strongly dependent upon the precise stacking sequence. Here we show that the electrostatic/polarization interaction provides a generic route to designing unprecedented, sizable and highly modulated (1 eV range), noncovalent on-tube potentials *via* encapsulation of inorganic partially ionic phases where charge anisotropy is maximized. Focusing on silver iodide (AgI) nanowires inside single-walled carbon nanotubes, we exploit the polymorphism of AgI, which creates a variety of different charge distributions and, consequently, interactions of varying strength and symmetry. Combined *ab initio* calculations, high-resolution transmission electron microscopy, and scanning tunneling microscopy and spectroscopy are used to demonstrate symmetry breaking of the nanotube wave functions and novel electronic superstructure formation, which we then correlate with the modulated, noncovalent electrostatic/polarization potentials from the AgI filling. These on-tube potentials are markedly stronger than those due to other noncovalent interactions known in carbon nanotube systems and lead to significant redistribution of the wave function around the nanotube, with implications for conceptually new single-nanotube electronic devices and molecular assembly. Principles derived can translate more broadly to relating graphene systems, for designing/controlling potentials and superstructures.

KEYWORDS: carbon nanotube hybrids · scanning tunneling microscopy/spectroscopy · symmetry breaking · electronic superstructure · electrostatic/polarization interaction · AgI@SWCNT · density functional calculations

Templated confinement in carbon nanotubes has emerged in recent years as a successful route toward producing low-dimensional hybrid nanomaterials[1] with new and diverse nanoscale properties and applications. These range from nanochemistry vessels[2] and attogram mass transport,[3] to sensitive chemical sensors,[4] to transport phenomena, such as negative differential resistance (NDR)[5] or spin-based, for quantum information,[6] or vectors for drug delivery.[7] Templated confinement also generates phases of materials that are otherwise inaccessible. In particular, in single-walled carbon nanotube (SWCNT) hosts, confinement reaches extreme levels, down to single-molecule[8,9] or even single-atomic rows.[5,10,11] Effects are particularly rich when confining inorganic materials with theoretical predictions and increasing experimental evidence of unique morphologies inside SWCNTs: inorganic nanotubes,[12] twisted structures,[13] with reduced symmetry and high anisotropy.[13,14] Furthermore, SWCNT confinement can result in diameter-controlled polymorphism of encapsulated inorganic material.[10]

This large variety of nanostructures has provided us with a set of archetypal interactions through which it is possible to modify the host nanotube to produce new functionalities and control nanotube behavior. These, however, have limitations: hybridization can strongly degrade nanotube's most desirable properties and is not preferred;[15] noncovalent interactions with molecular systems are weak, with at most ~0.2 eV potential modulation at the nanotube's walls, as reported for metallocenes inside semiconducting SWCNTs,[16] while the π-stacking interaction of aromatic planar molecules is even weaker, leading to only minor perturbations in the nanotubes;[17] meanwhile, the interlayer interactions in double- or multiwalled carbon nanotubes depend strongly on the precise stacking sequence and are not entirely noncovalent but partially involve hybridization.[18]

In contrast, confined inorganic compounds can influence carbon nanotubes in ways that are distinctive yet little explored

* Address correspondence to a.ilie@bath.ac.uk.

Received for review August 27, 2010 and accepted March 2, 2011.

Published online March 03, 2011
10.1021/nn102189w

to date. This is the core idea we explore here. We pose the question: can inorganic nanostructures produce potentials that combine the best characteristics of archetypal interactions but without their limitations; that is, can they be made noncovalent but strong and can they be tailored (in magnitude and spatial distribution) through design? Some evidence already exists in relationship to the inorganic systems described above. Symmetry lowering in an encapsulated inorganic structure can make the nanotube cross section oval; this was observed in high-resolution transmission electron microscopy (HRTEM) for a double tetrahedral chain of CoI_2,[13] or inferred[19] and then theoretically confirmed for ribbon-like AgI in very narrow nanotubes.[14] Further, polarization-induced modulation of the electrostatic potential at the nanotube cage was invoked to explain NDR transport in SWCNTs with KI filling.[5] These examples support the hypothesis that noncovalent interactions from compounds with a degree of ionicity can significantly affect the encapsulating nanotube. One can further envisage that, as encapsulated inorganic structures can be formed with regulated, "quantized" number of atomic rows, they could result in interaction potentials that are unique in strength and geometry, where symmetry can be controllably modulated, with potentially important implications for electronic transport and molecular assembly.

To explore these possibilities, we chose to work with AgI on account of its especially rich bulk phase diagram:[20] at ambient conditions, it crystallizes as coexisting zinc blende (γ-AgI) and wurtzite (β-AgI) phases; at 147 °C, it transforms to a superionic phase (α-AgI) of very high ionic conductivity, while at increased pressure, the rock-salt phase occurs. Very recently, it has also been shown that confinement into quasi-spherical nanoparticles of decreasing size, down to 11 nm, results in a phase transition to superionicity which, remarkably, then persists even down to room temperature.[21] A further practical advantage was that we could obtain AgI-filled SWCNTs in high yield. Thus AgI is prefigured as an ideal polymorphic material at the nanoscale, where nanophases with very different arrangements of cations and anions can be achieved. We exploit these here as model systems to demonstrate the design of noncovalent, sizable, modulated on-tube potentials arising from well-chosen charge distributions.

Further, if we want to use such nanophases to control the on-tube nanotube potential, we need to be able to correlate their structure, physical properties, and/or functionality down to the *atomic level*. To date, there are virtually no atomic level investigations of the electronic changes induced in SWCNTs by confined inorganic materials—yet at such a degree of confinement, small conformational changes can have substantial effects. Previous attempts to locally characterize functionality in hybrids of SWCNTs and inorganic compounds are scarce[3,5,22] (adding to just a few studies on metal-filled MWCNTs)[23] and not at the atomic level, in contrast to their counterparts involving molecular systems.[8,24−27] To fill this gap, our study of polymorphic AgI nanophases encapsulated in SWCNTs therefore combined atomic-resolution scanning tunneling microscopy/spectroscopy (STM/STS), HRTEM, and *ab initio* calculations. STM (and associated STS) is a local characterization technique that can directly probe the interplay between an encapsulated material and its nanotube host. Previous application has only been to molecular systems, which hybridize with nanotubes (such as encapsulated fullerenes)[8] or have mixed interactions, such as van der Waals and interlayer hybridization (in double- and multiwalled carbon nanotubes),[18] or $\pi-\pi$ stack (*e.g.*, small aromatic species[25] and macromolecules).[26,27]

In this work, we propose and show evidence of the capability of inorganic nanostructures to be unique sources of strongly modulated (1 eV range) noncovalent potentials, where symmetry can be controlled through the phase of the encapsulated filling. This is based on DFT *ab initio* predictions and on first-time observations through STM/STS of symmetry breaking of the nanotube's wave function and formation of a superstructure in AgI@SWCNTs, which we attribute to the partial ionic character of the filling. These observations are supported by an in-depth structural analysis of AgI nanophases from HRTEM. We thereby propose a generic route to designing sizable modulated, electrostatic/polarization, on-tube potentials by selecting encapsulated nanophases of inorganic compounds where charge anisotropy distribution is maximized. Such on-tube potentials produce strong wave function concentration around the nanotube that could be exploited in novel, single-nanotube "waveguide-like" devices and in controlling molecular assembly.

RESULTS

Key experimental observations (STM and HRTEM) were pursued using theoretical modeling and analysis, prompting further prediction. Central to the main concept of the work is the identification of two main crystallization classes adopted by AgI nanophases inside SWCNTs, one of which possesses a distinct separation of positive and negative charges, and another where opposite sign charges alternate, leading to a strong compensation of their influence. These charges derive from the partial ionic character of AgI, which tends to increase through confinement in SWCNTs. HRTEM enabled identification of the two classes. Theoretical modeling quantified the ionic character, allowed the polarization potential modulation induced at the nanotube wall to be estimated, and confirmed that the effect is robust enough to survive structural relaxation, with the main characteristics of the effect depending essentially on the primary crystallization, with relaxation inside specific nanotubes affecting only

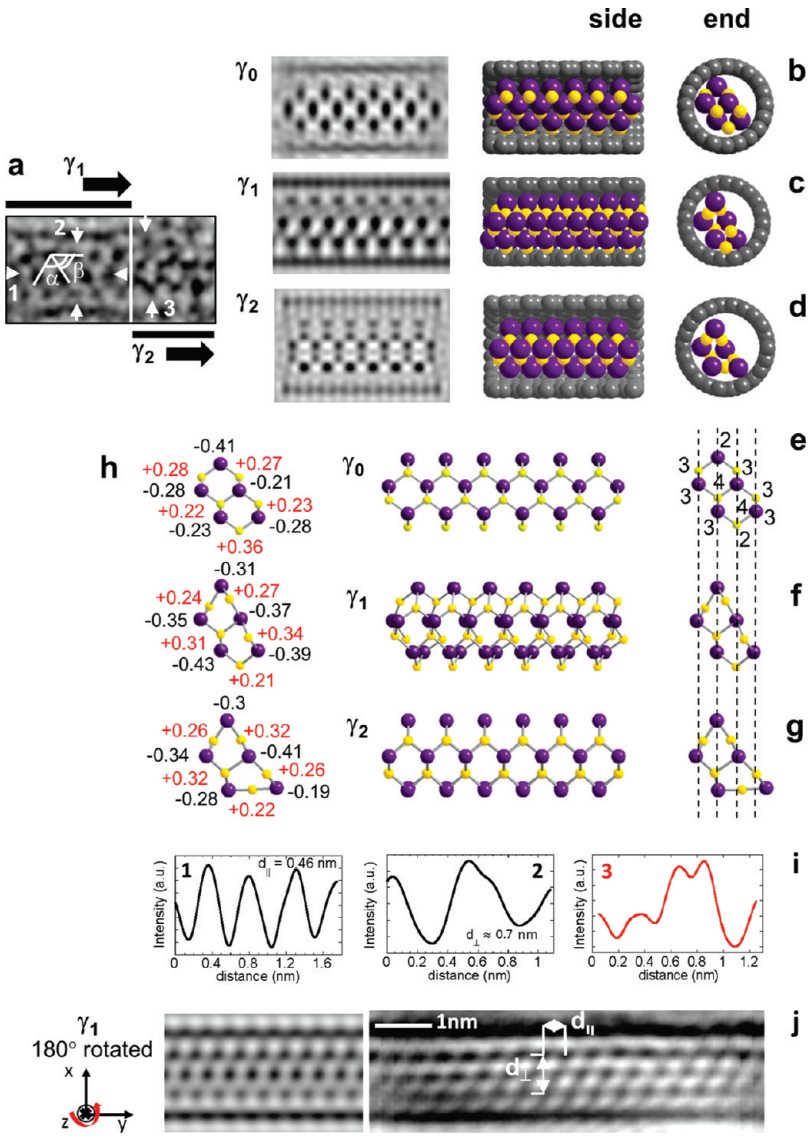

Figure 1. γ-AgI nanophases inside SWCNTs: γ_0, cut from bulk zinc blende, and its relaxations, γ_1 and γ_2. (a) HRTEM images (200 keV) for γ-type AgI nanowires inside nanotubes of diameters 1.5 nm (left, γ_1) and 1.64 nm (right, γ_2); (b) γ_0-AgI@(20,0)SWCNT. Right and middle: structural model of γ_0 (bulk zinc blende) AgI inside a (20,0) SWCNT in end and side views. Long axis is along the crystallographic axis ⟨011⟩ of bulk zinc blende AgI. Left: simulated TEM image. (c) γ_1-AgI@(20,0)SWCNT as obtained through DFT allowing both γ_0 and the (20,0) SWCNT to simultaneously relax. Right to left: end and side view structural models and simulated HRTEM image. (d) γ_2-AgI as obtained through DFT allowing γ_0 to relax in a (22,0) nanotube. Right to left: end and side view structural models of γ_2 inside nanotube and simulated HRTEM image. TEM simulations (b−d) use focal distance $D_f = -42$ nm. (e−g) Ball-and-stick models of γ_0, γ_1, and γ_2-AgI; in end view, the coordination number c for each ion/cation is marked. (h) Ionic charges for AgI found by performing Mulliken population analysis on DFT calculations. (b−h) Ag, yellow; I, purple. (i) Intensity profiles along directions 1−3 shown in (a). (j) HRTEM image (100 keV) for γ_1-type AgI inside a ∼1.5 nm diameter nanotube (right) and simulated image ($D_f = -44$ nm) based on DFT-relaxed structure (left).

the details. Theory also indicates that the modulation of the on-tube potential is large enough to be observed with the STM only for the AgI phases with significant charge separation (in the current case, zinc-blende-derived). STM measurements on AgI@SWCNTs reveal an electronic superstructure consistent with these theoretical predictions and are presented as an initial proof of the polarization potential modulation effects that we propose.

HRTEM Imaging and Simulations: Structure Assignment of Polymorphic AgI. We focus on AgI crystallized inside arc-discharge-grown nanotubes, that is, with diameters peaking at ∼1.4 nm (for AgI nanophases outside this range, see Supporting Information). Figures 1−3 show HRTEM images of two dominant AgI crystallizations we observe in this range, referred to as γ-type and β-type, and which exhibit a clear difference concerning their associated ionic charge distributions and concomitant induced on-tube potentials.

Assignment of the γ-Type Crystallization. This is based on a comparison of HRTEM images with image simulations of AgI zinc-blende-derived structures that

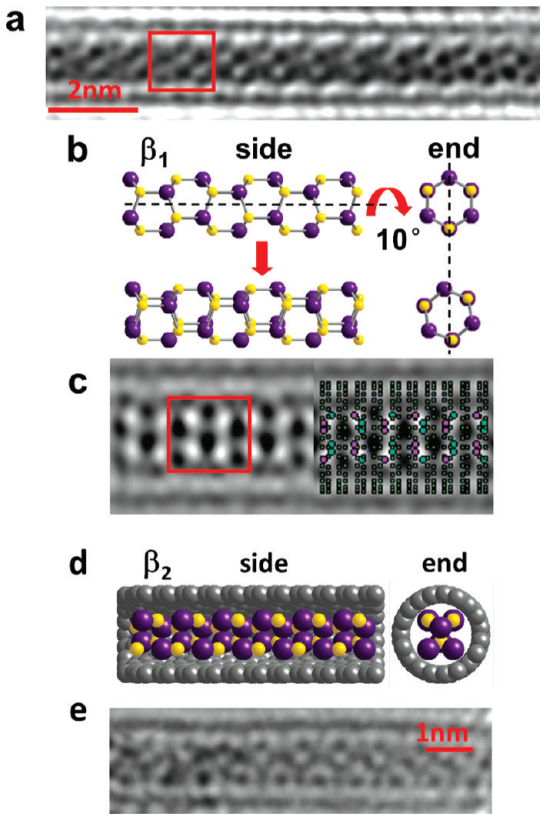

Figure 2. β-AgI nanophases inside SWCNTs. (a) HRTEM image (200 keV) of a β_1-AgI nanowire inside a SWCNT. (b) Structural model based upon β_1-AgI for two inclinations. End view is along the bulk crystallographic axis ⟨001⟩ of wurtzite AgI. (c) Simulated HRTEM image of β_1-AgI@(17,0)-SWCNT (left) with superimposed structural model (right). Focal distance D_f = 2 nm. A 1.3 nm diameter SWCNT is compatible with the black/white nanotube contours in the experimental image. Red squares in (a,c) highlight experimental/modeled repeat motif. (d) Structural model for an unrelaxed β_2-AgI@(19,0) SWCNT phase. End view is along the bulk axis ⟨001⟩ of wurtzite AgI. Everywhere, Ag is yellow Ag, I is purple. (e) HRTEM image (100 keV) suggesting a β_2-derived AgI structure inside a nanotube with diameter ≥1.5 nm.

were subjected to structural relaxations using DFT calculations and supported by the observation of the zinc blende phase in SWCNTs of increasingly wide diameter. Inside a nanotube diameter of about 1.5 nm, there is a first type of appearance, γ_1, as shown at left of Figure 1a and in 1j, on a length ≥7 nm. Projected periodicities (*i.e.*, as seen under the electron beam) are $d_{\parallel} \approx 0.46$ nm and $d_{\perp} \approx 0.7$ nm from line profiles 1 and 2 (Figure 1i), with angles $\alpha \approx 122°$ and $\beta \approx 55°$. These parameters span the ranges 0.455−0.47 nm, 115−122°, and 51−58°, respectively, as the nanotube diameters vary from 1.4 to 2 nm. Such values are close to distances and angles in bulk zinc blende AgI (where $d_{\parallel} \approx 0.46$ nm, $d_{\perp} \approx 0.65$ nm, $\alpha \approx 125°$, and $\beta \approx 55°$).[20] A second image type, labeled γ_2, appears at the right of Figure 1a and is characterized by transverse profile 3 (Figure 1i). The nanotube encapsulating γ_2 is larger, about 1.64 nm in diameter, than that encapsulating γ_1.

To further elucidate the structures in these HRTEM images, simulations based on proposed structural models (as opposed to image reconstruction techniques[13]) were performed (see Methods). Figure 1b,e shows a "γ_0" zinc-blende-based cut, that is, with bulk structural parameters. The atomic coordination number c of the central atoms retain the four-fold bulk coordination, while it decreases to either three or two for the most exterior ones, a reduction which, if unconstrained, is bound to promote structural relaxation. Using DFT calculations (see below), γ_0 was found to relax into γ_1 inside a (20,0) nanotube of 1.56 nm that was simultaneously allowed to relax (Figure 1f) and into γ_2 while in a larger (but also semiconducting) (22,0) nanotube (Figure 1g). In γ_1, the c = 2 Ag ion compensates for the low coordination environment by moving toward the nanotube, which itself slightly deforms in order to follow the contour of the AgI filling (see Discussion). This is a trend also documented in other relaxed nanotube systems.[10,13,14] On the contrary, in γ_2 the c = 2 Ag ion moves upward. Figure 1a−d compares HRTEM images with respective simulations from γ_0 (unrelaxed) and γ_1 and γ_2 (relaxed) structures: the overall agreement is improved for γ_1 in reproducing the left of Figure 1a, while the right side of Figure 1a is consistent with γ_2 inside the larger SWCNT. The success of the DFT-derived model in providing good matches to the experimental images demonstrates the viability of the originating zinc blende structures that were proposed.

Assignment of the ***β****-Type Crystallization.* This is based on image simulations using structural models derived from wurtzite AgI and validated by comparison with related published data.[28−30] Figures 2 and 3 show β-type crystallization of AgI: this is labeled as β_1 in nanotubes of 1.3 nm diameter (Figure 2a and 3) and as β_2 in nanotubes of ∼1.5 nm diameter (Figure 2e).

The β_1 structure in Figure 2a has a constant orientation over a 80 nm length (not shown), while that in Figure 3 appears to rotate along the nanotube axis by some 70° from left to right, where it reaches a similar appearance to that in Figure 2a. It also appears to be slanted (Figure 3b,c). Typical structural parameters obtained for this crystallization (Figure 3) are $d_{\parallel} \sim 0.8$ nm, $d_{\perp} \sim 0.48$ nm, and $\gamma \sim 135°$, close to bulk wurtzite AgI where $d_{\parallel} \sim 0.75$ nm, $d_{\perp} \sim 0.4$ nm, and $\gamma \sim 140°$.[20] A structural model for β_1, consistent with the inorganic nanotubes predicted in ref 12, and the related image simulation are shown in Figure 2b, c, respectively. Further validation for this proposed structure comes from ref 28, where a similar HRTEM image and proposal was made for a nanocrystal obtained through the encapsulation of a AgI−AgCl eutectic mixture.

The β_2 structure (Figure 2d) is closely related, though larger, to that of β_1, with both originating from wurtzite AgI. Its HRTEM image (Figure 2e) resembles AgI@SWCNT

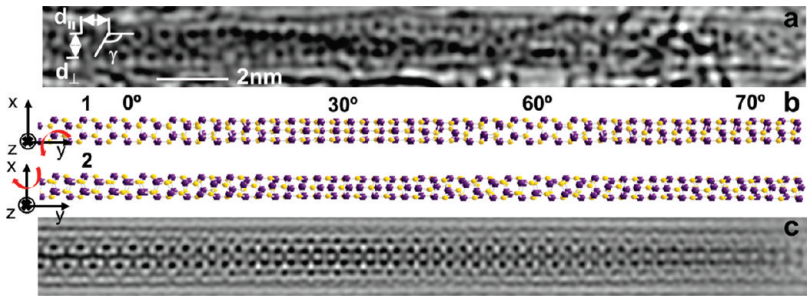

Figure 3. Encapsulated nanophases can rotate inside the host nanotube. (a) HRTEM image (200 keV) of a β_1-AgI nanowire; $d_\parallel$, $d_\perp$, and γ are characteristic projected periodicities and angles. (b) Model 1: 22 nm long section of β_1-AgI, with rotation $\varphi(y)$ applied around the nanotube axis at different segments, resulting in an overall rotation of $\Delta\varphi = 70°$. Model 2: obtained from model 1 applying a uniform additional 10° rotation around the *x* axis. Both models are approximations and not reconstructions from image (a). (c) Simulated HRTEM image using model 2 inside a 1.3 nm diameter (17,0) SWCNT. Focal distance $D_f = -15$ nm. Everywhere, Ag is yellow, I is purple. The central part of the real image appears as the overlap between the proposed model and another unidentified structure located in a different plane.

images reported in ref 29 and are analogous to CuI@SWCNT images and structure observed in ref 30, where both AgI and CuI share the same iodine network as backbone. Finally, as the HRTEM images are in good agreement with structural models of β_1 and β_2 put inside such nanotubes without relaxation, this suggests that, even if relaxation is expected in the real case, this would not significantly change the major features of the TEM images (unlike the γ structures above).

Scanning Tunneling Microscopy and Spectroscopy: Symmetry Breaking and Electronic Superstructure. Figure 4a,b shows an illlustrative set of STM images taken on AgI-filled SWCNTs at 77 K for different sample bias voltage V_s (positive, to favor nanotube, *i.e.*, sample, states)[31] and constant tunneling current. When V_s is decreased, the pattern familiar for unfilled SWCNTs that is visible at 3 V (and similar to Figure 7b) shows clear changes below 2 V, acquiring a stripe-like superstructure. Its stripes are incommensurate with the nanotube, inclined at a small angle relative to the nanotube axis, and rotate slightly along its length, while the nanotube itself does not have a twist. They also do not fade away in overall intensity along the nanotube, as occurs due to scattering from defects on walls.[32,33] Several motifs evolve from one into the other along the axis, with higher intensity regions, about four C−C bonds wide, separated by lower intensity regions in the azimuthal direction. Typically, about two such stripes are accommodated across the face of the nanotube, while along the nanotube axis there is a periodicity of about 5 nm. Notably, the stripes stay in the same place and with similar gross features, while the bias is varied over a large range, ∼1 eV, thereby ruling out interference effects from small momentum scattering which would cause phase randomization and result in highly energy-dependent features as observed in both supported[34] and unsupported SWCNTs.[35] Other superstructures commonly identified on SWCNTs[33,36,37] (as well as on graphite and MWCNTs[38,39]) have a $(\sqrt{3} \times \sqrt{3})R30°$ symmetry relative to the original, unperturbed SWCNT lattice. These originate from large momentum (Umklapp) scattering involving defects or natural ends of nanotubes and usually decay over ∼5 nm.[32,37] Depending on the various phases accumulated by the wave function after scattering, the exact pattern of the $\sqrt{3}$ superstructure can vary.[37] Other systems closer to our case, such as the peapod nanotubes with encapsulated metallofullerenes, have shown strain effects reflected in both a $(\sqrt{3} \times \sqrt{3})R30°$ fading superstructure in topographic images and a band gap modulation in conductance d*I*/d*V* images.[8] Both effects were attributed to variable elastic strain around the fullerene-filled regions. Small angle bends such as that in Figure 4 do not backscatter electrons[40] and have a negligible effect on the nanotube electronic structure,[41] as confirmed by site-dependent STS taken above and below the bend.

Combining imaging with STS (Figure 4a,d) has allowed us to assign the SWCNT probed: (i) the presence of low energy peaks in the tunneling density of states (DOS) indicates a semiconducting nanotube; (ii) after lattice contraction to eliminate the tip size effect,[42] a chirality $\theta \sim 5-6°$ (defined relative to the zigzag direction) was determined; (iii) the position of DOS peaks in STS suggests a (18,2) SWCNT (of $n - m = M(3) + 1$ type), which matches well the theoretical LDA-DFT DOS for this type of tube from ref 43 (see Figure 4d). The DOS of another candidate, the (19,2), a $n - m = M(3) - 1$ nanotube agrees less well. The STM pattern obtained at constant current (Figure 4a, panels 1 and 2) could differentiate between the $M(3) \pm 1$ nanotube varieties based on image calculations available in the literature[44] but only at low energy, around the first unoccupied/occupied van Hove singularities, when one does not average states of various symmetries[44,45] like here. However, this pattern is consistent with low chirality SWCNTs, where there is asymmetry between the bonds closely aligned with the nanotube axis and the ones across it (ref 44 and Figure 7b). An (18,2) tube has a diameter of ∼1.5 nm, sufficient to accommodate many of the AgI structures described above. In this interpretation, theoretical and experimental DOS differ primarily through a global

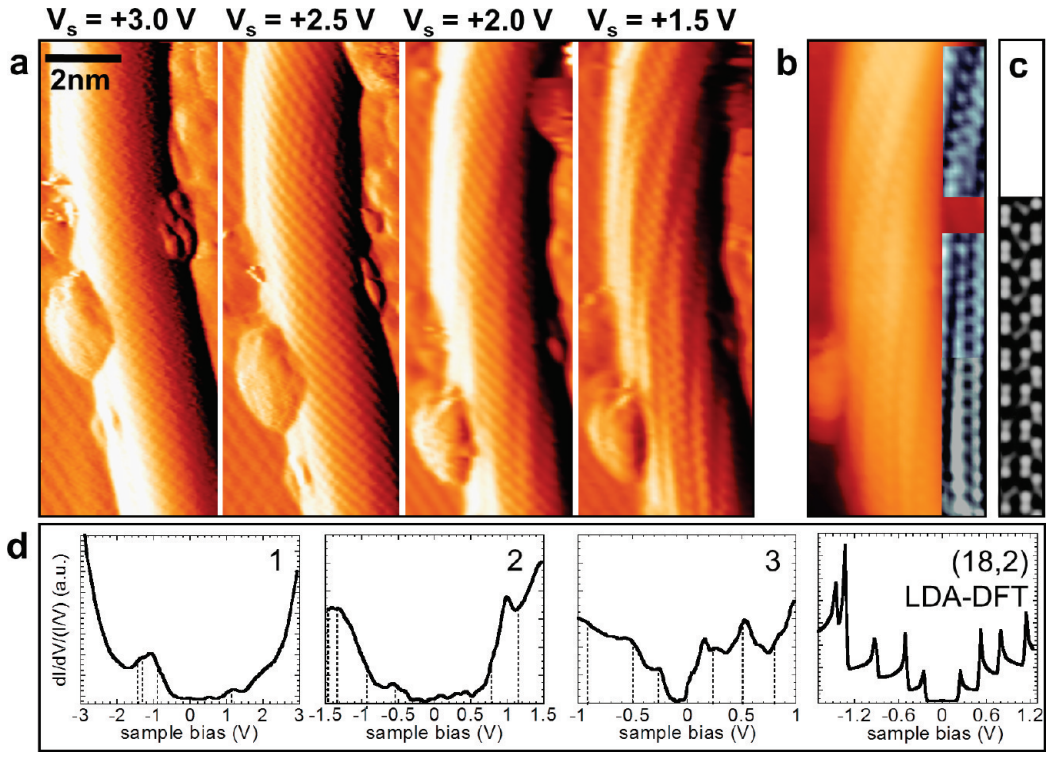

Figure 4. STM images of AgI@SWCNT showing stripe-like electronic superstructure, and associated STS. (a) Constant current (I = 0.5 nA) STM images at varying sample bias V_s; shown before contraction to eliminate tip size effects. Image derivatives are used for enhanced topographic contrast. Clusters around the nanotube are attributed to amorphous carbon which is known to only interact very weakly with nanotubes. (b) Real topographic image measured at V_s = +1.5 V (left) and after removing the parabolic profile of the nanotube (right); the latter corresponds to the center of the image. (c) Simulated STM image showing broken symmetry of the usual SWCNT pattern (part of Figure 7a) for qualitative comparison with (b). (d) (dI/dV)/(I/V) normalized STS curves over three distinct voltage ranges (panels 1−3). Sweeps were taken between $+V_s$ and $-V_s$, with V_s the bias used for imaging, and at progressively lower tip−surface distances resulting from the condition I = 0.5 nA. For panels 1 and 2, this resulted in unrealistic nearly zero density of states at low energies. Panel 4 shows LDA-DFT DOS of an (18,2) SWCNT (from ref 43). Dashed lines on panels 1−3 mark the van Hove singularities of this theoretical DOS. For each V_s range, two series of site-dependent spectroscopic curves were taken, each at 10−15 points along the nanotube axis. The spectroscopy is representative of sites on the nanotube axis.

broadening of experimental peaks compared to theory and a more pronounced mismatch in the 0.7−1.2 eV region where the theoretical peak at ∼0.8 eV disappears, and instead, there is broadening of the experimental resonances centered at 0.6 and 1 eV. This suggests a large level repulsion, which we show below is possible, and indeed expected, in nanotubes filled with γ-AgI phases.

DISCUSSION

Changes in Electronic Structure and Phenomena at the Walls. STM images suggest the origin of the stripe-like superstructure to be a *long-range potential* (*i.e.*, varying over at least several bond lengths, as opposed to atomic scale[46]), expected to affect semiconducting SWCNTs,[46] of which an obvious source is the ionic potential from the encapsulated AgI nanowires. We argue this idea below, in two stages. First we have examined the on-tube electrostatic potential modulation induced by AgI nanostructures using DFT calculations for a small number of systems and, more generally, using the discrete dipole approximation (DDA), for which we allocate partial ionic charges to each anion/cation as identified from Mulliken population analysis (MPA) in the DFT results. Then we used the knowledge acquired regarding the symmetry of the on-tube potential in simple phenomenological calculations (using tight-binding) in order to correlate the DOS on tube (calculated as $|\Psi|^2$) with the STM images. In doing so, we elucidate the general mechanism through which such a potential couples with the nanotubes.

On the basis of size (see left of Figure 1a and Figure 2d), both β- and γ-AgI phases can *a priori* form inside 1.5 nm SWCNTs as in Figure 4. However, there is a clear difference between the two concerning the associated ionic charge distribution. This is revealed by "unrolling" the whole AgI/nanotube system around the axis of the tube (Figure 5), a procedure that highlights Ag and I distributions relative to the originating graphene sheet. While in β structures the ions and cations alternate both axially and azimuthally (Figure 5c, d), in γ structures, they separate into axial rows containing only either positive or negative charges, with varying separation from one another and from the C

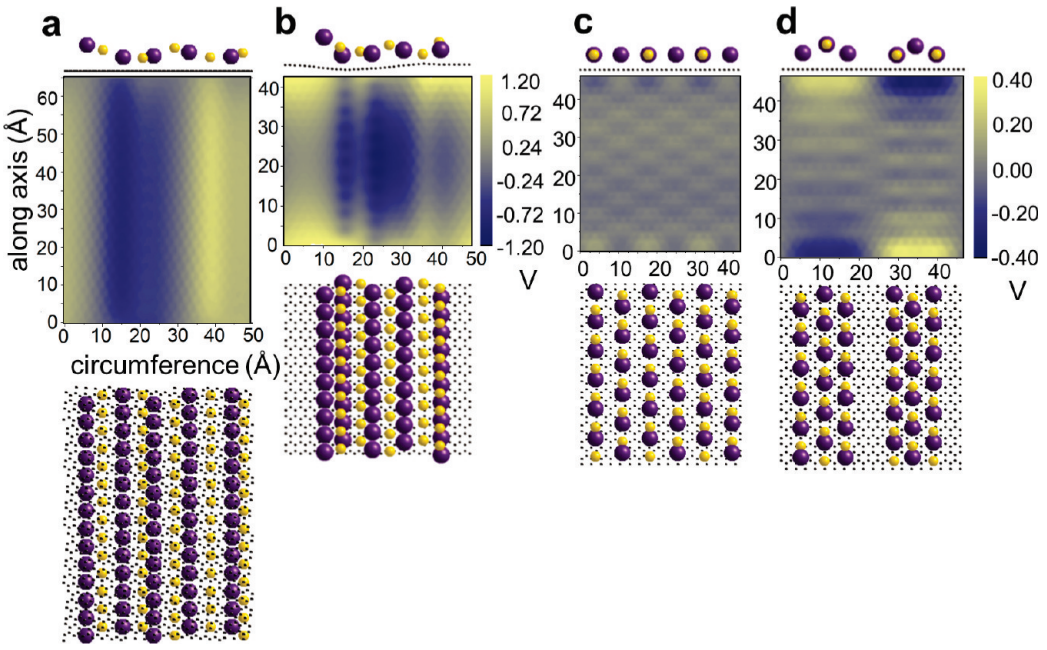

Figure 5. Maps of electrostatic potential on the unrolled graphene sheet (from unrolling AgI@SWCNTs around the tube axis) calculated using discrete dipole approximation, corresponding to the zinc-blende- (a,b) and the wurtzite-derived (c,d) structures: the γ phases induce the strongest potential, with a highly anisotropic, azimuthal dependence. (a) γ_0-AgI@(19,2)-SWCNT; (b) fully relaxed γ_1-AgI@(20,0)SWCNT, also showing nanotube deformation; (c) β_1-AgI@(17,0)SWCNT; (d) β_2-AgI@-(19,0)SWCNT. Note (a,b) use a different scale to (c,d), where variations are smaller. For each case, top and lower panels are end and side views of the unrolled structural models. Everywhere, Ag is yellow, I is purple.

atoms (Figure 5a,b). Figure 5 also shows the on-tube modulation of the electrostatic potential induced by these charges obtained within the DDA model (implemented as in ref 5). For this, we associated an induced atomic dipole with each C atom characterized by an anisotropic polarizability tensor $\vec{\alpha}_C$.[47] For the γ structures, our MPA gave charges with magnitude of $\pm 0.2e - \pm 0.4e$ on the Ag and I atoms (Figure 1h) and $\sim \pm 0.3e$ for β structures (not shown), consistent with the partial ionic character of AgI.[20] Figure 5c,d shows that β structures can be ruled out as the origin of the stripes seen in the STM images: the rapidly oscillating potential (with $\sim$0.7 nm period) along the nanotube's axis cannot induce linear features as seen in the experiment. In contrast, the potential generated by the γ structures (Figure 5a,b) is consistent with STM: along the axis of the tube, stripes of constant sign occur, leading to an essentially *azimuthal* variation of $\sim 1-1.3$ eV amplitude. Variations this large are expected to strongly affect the nanotube electronic structure but should not be felt directly by the tip during constant current tunneling at usual tunneling distances.[48] In contrast, for the β-AgI structures, on-tube potential variations are much smaller, of $\sim 0.1-0.2$ eV (Figure 5c,d).

To pursue this idea, DFT simulations were performed (see Methods and Computational Details and Supporting Information). Related AgI@SWCNT systems, that is, the unrelaxed γ_0-AgI@(20,0) SWCNT (Figure 1b,e) and the fully relaxed γ_1-AgI@(20,0) SWCNT (Figure 1c,f), were chosen instead of the (18,2) nanotube observed with STM in order to keep the overall calculation cells to a manageable size. The on-tube electrostatic potential for the β_1-AgI@(17,0) SWCNT was also calculated (see Methods and Computational Details). For all three systems, the on-tube electrostatic potentials from DFT and DDA agree well in magnitude (Figures 5 and 6; Methods and Computational Details). This validates DDA as a viable method for revealing potential modulations in nanotube structures of larger size (such as the chiral SWCNT from Figure 5a), for which first principle calculations are not available.

We then analyzed by DFT changes obtained in the energy band structure of the relaxed system γ_1-AgI@(20,0) SWCNT compared to the unperturbed (20,0) SWCNT and the unrelaxed γ_0-AgI@(20,0) SWCNT, the partial density of states (pDOS) of both nanotube and AgI, as well as the spatially resolved electrostatic potential and local DOS (LDOS) around the nanotube's circumference. We summarize the main results (see Supporting Information for details): (1) AgI produces a significant electrostatic potential modulation at the nanotube wall, which reaches ≈ -1 eV (attractive) on the side where the c = 2 Ag atom relaxes toward the tube, and $\approx +0.3$ eV (repulsive) on the opposite side (Figure 6b). (2) The filling induces a small nanotube deformation (Figure 1b,c and Supporting Information), but this does not account for the changes in its electronic structure. (3) Hybridization between AgI and nanotube can also be discounted as an origin of the

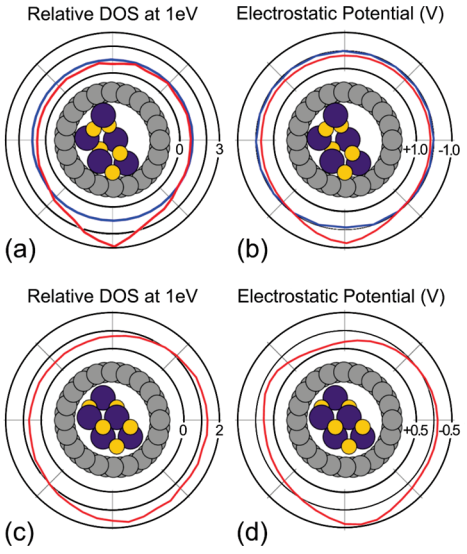

Figure 6. Local density of states (LDOS) reorganizes anisotropically around the nanotube due to the strong azimuthal dependency of the on-tube electrostatic potential. (a) Calculated LDOS at 1 eV above E_F on C atoms around the nanotube in the fully relaxed γ_1-AgI@(20,0)SWCNT system, divided by the corresponding DOS on the ideal (20,0) SWCNT (red), showing a strong enhancement in the vicinity of the protruding Ag ion. In the same place, the relaxed SWCNT has a small distortion. The same DOS quantity for a similarly distorted, but unfilled (20,0) SWCNT (in blue) is almost constant around the tube. (b) Calculated electrostatic potential (negative corresponds to attractive to electrons) around the circumference of the filled nanotube (red) and empty distorted nanotube (blue). (c,d) Corresponding results to (a,b) for the unrelaxed γ_0-AgI@(20,0)-SWCNT system.

large electronic structure changes which result instead from the *AgI polarization potential*, as initially proposed. These changes are mainly due to energy level mixing within a large energy window caused by the large electrostatic potential which result in *broad level repulsion*; in addition, smaller level splittings occur due to a lifting of degeneracy with the filling breaking mirror symmetry of the (20,0) nanotube. We find all changes are consistent with couplings induced by terms in a Fourier development of a potential $U(\varphi) = \sum_m U_m \cos(m \times \varphi + \chi_m)$, which expresses the azimuthal (φ) dependency noted with DDA. The individual terms account for the mixing and subsequent repulsion of nanotube energy levels with azimuthal quantum numbers[49] q and q' where $|q - q'| = m$, within an energy window of $\sim U_m$. For γ_1-AgI, the magnitude of U_m means this selection rule effectively mixes levels with $|q - q'| \leq 4$ separated by up to a few tenths of electronvolts. (4) Significantly, we observe a clear correlation between the local DOS on the nanotube and the electrostatic potential (Figure 6a,b): around the $c = 2$ Ag atoms, where the induced potential is most attractive, the LDOS increases by about 200% and is decreased where the induced potential is repulsive. Thus, there is *substantial wave function redistribution around the nanotube*. Importantly, *all of these trends in the electronic structure changes are general, independent of the degree of relaxation of* γ-AgI as proved by similar calculations performed, for example, on the unrelaxed γ_0-AgI@(20,0) SWCNT system (Figure 6c,d). Here the potential is more regularly oscillatory, resulting in relatively stronger contributions from higher m components of U. For the β_1-AgI@(17,0) SWCNT, the potential behaves differently (as obtained also with the DDA model): it exhibits approximately three-fold rotationally symmetric variations with amplitude $\sim$0.1 eV at the wall of the nanotube, which change polarity every $\sim$0.4 nm along the tube axis. The consequence is much less pronounced variations in the electronic structure of the nanotube.

To further connect with the experiment, we used the tight-binding approximation to study how the SWCNT's wave functions are affected by a generic perturbing potential $U = U_m \cdot \cos(m \times \varphi + \delta\varphi(y))$, where $\delta\varphi(y)$ describes a slow twist angle along the y axis of the tube (see Supporting Information). We assume this slow y dependence of U leaves k along the tube[49] axis a good quantum number and consequently does not cause mixing of states with different k (see Supporting Information). Figure 3 suggests that such "twists" are possible, in addition of having been observed in other inorganic or monatomic fillings.[10,13] We do not aim here for an exact replication of the features of our STM images, but an explanation that captures the essential phenomena. For this, we chose $m = 6$ to account for the faster azimuthal modulations of our images and for simplicity the achiral (19,0) semiconducting nanotube close in diameter to the (18,2) in the experiment. The $m = 6$ value corresponds to a more compact γ-AgI structure, expected to form inside a narrower nanotube, such as the (19,0), and which promotes a more azimuthally isotropic relaxation. Figure 7 shows how U_6 mixes the $q,q' = 6,12$ states: the resulting $|\Psi|^2$ (Figure 7a) breaks the symmetry of the usual STM patterns of the unperturbed nanotube (Figure 7b,c) by (i) acquiring a stripe-like superstructure which (ii), due to the $\delta\varphi(y)$ rotation, slowly changes along the axis of the tube, with a period of a few nanometers. This replicates the essential features of the experimental images, though not their exact pattern (Figure 4b,c). In ongoing work, we are extending our DFT studies by including the full perturbing potential and allowing k mixing. As shown in ref 50, helical potentials can affect semiconducting SWCNTs.

Finally, we comment on the magnitude and spatial variation of the on-tube polarization potentials one could induce by encapsulating (partially) ionic compounds: our study shows that these parameters can be tailored by appropriately choosing the compound and its phases. In particular, the >1 eV on-tube potential from our γ-AgI nanowires is substantially larger than other potential modulations induced by various encapsulated molecules (*e.g.*, $\sim$0.2 eV from metallocenes inside

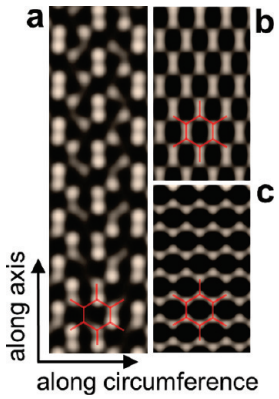

Figure 7. On-tube potentials with anisotropic variation provide a general mechanism for electronic superstructure and wave function reorganization to occur. (a) Calculated STM image (as $|\Psi|^2$) showing symmetry breaking in a (19,0) SWCNT due to an azimuthal potential with $m = 6$, *i.e.*, $U = U_6\cos(6\varphi + \delta\varphi(y))$. The two lowest energy unoccupied bands of the unperturbed nanotube (q,q' = 6,12) at an energy ~0.8 eV and $k \approx 0.1$ Å^{-1} have been mixed. The resulting pattern mixes axial rows with more and less pronounced bonds. The y twist in the potential means that bond prominence/appearance can also vary periodically along an axial row, with some bonds being only partially visible (see also Supporting Information). (b,c) $|\Psi_q|^2$ for $q = 6$ and 12, the lowest two unoccupied energy bands of the unperturbed, unfilled nanotube, respectively. For small chiral angles (here, $\theta = 0°$), there is asymmetry between the bonds aligned with the nanotube axis as opposed to the ones across it.

semiconducting SWCNTs)[16] or, even more so, compared to the π-stacking interaction of aromatic planar molecules (which only led to minor perturbations in the nanotubes).[17] Devices with individual SWCNTs partially filled with potassium iodide (KI) nanocrystals showed negative differential resistance (NDR), which was attributed to electrostatic potential modulation on the nanotube of ~0.2−0.3 eV caused by permanent dipoles in the KI chain.[5] Further, we note that the polarization interactions we demonstrated here are different than the interlayer interaction encountered in double- or multiwalled carbon nanotubes: the latter is not purely noncovalent, but partially caused by interlayer hybridization leading to disruptive changes such as semiconductor-to-metal transitions.[18] Significantly, in our case, the nanotube's character is preserved (see also Supporting Information).

CONCLUSIONS

To conclude, we have proposed that sizable on-tube potential modulations, in the 1 eV range, can be induced by the encapsulation of partially ionic AgI nanowires inside SWCNTs and presented initial evidence of their effects. The proposal is strongly rooted in theoretical modeling and predictions and supported by results from both HRTEM and STM/STS experiments. Symmetry breaking resulting in an electronic superstructure (observed with STM) and sizable electronic changes (such as wave function concentration and redistribution) occur and have been shown to not originate from either filling-induced strain fields or hybridization between AgI and nanotube states. Instead, this interaction potential is found to be predominantly of *ionic/polarization origin*, indicating that such noncovalent interactions, previously unexplored, can impact significantly and in novel ways upon nanotube properties.

Our results show that key to designing sizable, modulated, on-tube polarization potentials is a *strong charge distribution anisotropy* within the encapsulated inorganic nanostructures. This anisotropy is much greater in the zinc-blende-derived AgI nanowires than in the wurtzite-derived ones we identified, where the ionic charge distribution is more checkerboard in nature and most likely larger than in higher ionicity metal halides (such as KI) with rock-salt phase, although relaxation effects must also be considered.

The yield of AgI-filled SWCNTs is high, pointing to practical importance of our case study. Furthermore, the generic nature of our conclusions suggests other compounds may be similarly exploited; for example, Cu halides crystallize to zinc blende in bulk[20] and also fill SWCNTs with good yield.

Thus on-tube modulated polarization potentials can be considered a new addition to the body of effective interactions available in hybrid and functionalized carbon nanotubes for designing novel applications. As shown here, they can be made stronger than other noncovalent interactions encountered in hybrid nanotube systems, particularly those involving molecular systems, as well as provide an alternative to the interlayer/stacking interactions that are currently a focus in research on double- (multi-) walled carbon nanotubes or double- and few-layer graphenes. The significant anisotropic reorganization of the wave function they induce around the nanotube offers exciting possibilities for new single-nanotube "waveguide-like" devices, and in molecular assembly. Further, principles exposed here could impact more broadly, for example, in graphene electronics (and other layered, inorganic 2D materials) where there is an active interest in designing/controlling potentials and superstructures.

METHODS AND COMPUTATIONAL DETAILS

Synthesis of AgI@SWCNTs. AgI nanowires were formed inside SWCNTs from molten phase using established procedures,[19] in several nanotube diameter distributions (HiPCO, arc-discharge, Nanocyl), that is, centered around 1, 1.4, and 2 nm diameter, respectively. Filling yields between ~60 and 90% were

obtained, with the yield roughly increasing with increasing diameter.

HRTEM Imaging and Simulation. The images presented are representative of a substantial image bank from both 200 and 100 keV beam energies (taken with three JEOL microscopes, 2000, 2100F, and 3000F). At 200 keV, images were taken over a few seconds to avoid AgI evolution, and those showing evidence that this occurred were discarded. Energy-dispersive X-ray spectroscopy (EDX) on the medium and large diameter distributions of nanotubes confirmed that the encapsulated compound was AgI.

For image simulations, zinc-blende- and wurtzite-derived AgI models were obtained from the respective bulk crystals by cutting appropriately sized, electrically neutral slices, to fit inside the nanotubes. CrystalMaker[51] was used for this, incorporating rotations and inclinations for either components or whole structures. Resulting models were imported into the NCEMSS software,[52] and focal series were simulated when attempting to assign models to experimental images. Care was taken for images not at the Scherzer focus to assign the correct black/white contours for the SWCNT walls, in order to correctly determine tube diameters.

STM/STS. AgI@SWCNTs from dispersions in dichloroethane were dispersed on Au(111) substrates and annealed further in UHV to remove contaminants. STM/STS were taken with an Omicron LT-STM on AgI-filled SWCNTs at 77 K. Images showing signatures of nanotube defects were discarded.

Related but not identical STM features were obtained on a number of observed AgI@SWCNTs hybrids; it is expected the AgI structure inside nanotubes of varying diameters to depend on the degree of relaxation achieved. Images shown were processed with the WSxM software.[53] Feenstra's procedure[54] was used for the $(dI/dV)/(I/V)$ normalization. Images were very stable, unchanged even after V_s was cycled several times and after several tens of rounds of site-dependent spectroscopic curves had been taken along the nanotube (and also on clean Au(111)). This confirmed very good tip stability and ruled out tip-related effects. We started imaging from high to low bias in order to protect the tip from potential changes due to the higher incidence of debris when working with hybrids of nanotubes and inorganic compounds.

DFT *Ab Initio* Calculations (Further Details in Supporting Information). DFT simulations were performed using the CRYSTAL06 code.[55] Following Catti,[56] for AgI, we used the B3LYP hybrid functional, with Ag described using a Hay−Wadt small core pseudopotential for the $[Ar]3d^{10}$ core and a 311(sp)31(d)G basis of localized orbitals for the outer electron states, and I described using a Hay−Wadt large core pseudopotential for the $[Kr]4d^{10}$ core and 8 atomic orbitals of type 31(sp)G for the outer electrons. Gaussian parameters were the optimized set due to Catti.[57] For C, we used a 6-21G* basis, which yields a graphene lattice parameter of 2.5 Å.

Short-period commensurate models of encapsulated AgI nanowires have been studied. As an example, Supporting Information shows the calculated electronic structure for both a fully relaxed and unrelaxed γ-AgI nanowire contained within a (20,0) SWCNT ($d_{\|}$ = 0.43 nm; tube diameter 1.56 nm), that is, the γ_1- and γ_0-AgI@(20,0)SWCNT systems, respectively, from which the perturbing influence of the ionic filling can be recognized. Structural relaxation in a larger but also semiconducting (22,0) SWCNT ($d_{\|}$ = 0.43 nm; tube diameter 1.7 nm) was similarly performed and yielded the γ_2-AgI structure. In constructing these commensurate systems, the γ-AgI has been compressed in the direction along the tube by around 7%, which will have some effect on the resulting atomic positions. Therefore, we focus on the general characteristics of the system, which we expect will persist in more realistic structural models. More extensive calculations are currently being undertaken.

Similar calculations on a wurtzite-derived β-AgI@(17,0)SWCNT system have been performed using a structural model comprising 7 CNT and 4 AgI repeat units in the unit cell (524 atoms). In this case, the alternating arrangement of anions and cations along the tube axis leads to a more complex, checkerboard, variation in the electrostatic potential, and not the mainly linear variation that exists along the tube in the case of γ-AgI structures.

Tight-Binding Calculations. Technical details in Supporting Information.

Acknowledgment. A.I. wishes to thank Dr. A. N. Khlobystov for some of the 100 keV HRTEM images. This work was supported by EPSRC UK research Grant EP/G001707/1 and the International Cooperative Research Project (ICORP) of the Japan Science and Technology Agency. Computations were performed on the University of Bath High Performance Facility. Some HRTEM was provided through EPSRC UK research Grant EP/F01919X/1.

Supporting Information Available: Phase diagram of AgI@SWCNTs on the 0.7−5 nm range from HRTEM; DFT first principles calculations of AgI@SWCNTs; tight-binding theory with perturbative interaction potential. This material is available free of charge *via* the Internet at http://pubs.acs.org.

REFERENCES AND NOTES

1. Monthioux, M.; Flahaut, E.; Cleuziou, J.-P. Hybrid Carbon Nanotubes: Strategy, Progress, and Perspectives. *J. Mater. Res.* **2006,** *21*, 2774–2793.
2. Wang, Z. Y.; Shi, Z. J.; Gu, Z. N. New Phenomena of Materials Confined in Nano Space. *Prog. Chem.* **2009,** *21*, 2435–2444.
3. Costa, P. M. F. J.; Golberg, D.; Mitome, M.; Hampel, S.; Leonhardt, A.; Buchner, B.; Bando, Y. Stepwise Current-Driven Release of Attogram Quantities of Copper Iodide Encapsulated in Carbon Nanotubes. *Nano Lett.* **2008,** *8*, 3120–3125.
4. Brahim, S.; Colbern, S.; Gump, R.; Grigorian, L. Tailoring Gas Sensing Properties of Carbon Nanotubes. *J. Appl. Phys.* **2008,** *104*, 024502.
5. Ilie, A.; Egger, S.; Friedrichs, S.; Kang, D.-J.; Green, M. L. H. Correlated Transport and High Resolution Transmission Electron Microscopy Investigations on Inorganic-Filled Single-Walled Carbon Nanotubes Showing Negative Differential Resistance. *Appl. Phys. Lett.* **2007,** *91*, 253124.
6. Warner, J. H.; Watt, A. A. R.; Ge, L.; Porfyrakis, K.; Akachi, T.; Okimoto, H.; Ito, Y.; Ardavan, A.; Montanari, B.; Jefferson, J. H.; *et al.* Dynamics of Paramagnetic Metallofullerenes in Carbon Nanotube Peapods. *Nano Lett.* **2008,** *8*, 1005–1010.
7. Hong, S. Y.; Tobias, G.; Al-Jamal, K. T.; Ballesteros, B.; Ali-Boucetta, H.; Lozano-Perez, S.; Nellist, P. D.; Sim, R. B.; Finucane, C.; Mather, S. J.; *et al.* Filled and Glycosylated Carbon Nanotubes for *In Vivo* Radioemitter Localization and Imaging. *Nat. Mater.* **2010,** *9*, 485–490.
8. Lee, J.; Kim, H.; Kahng, S.-J.; Kim, G.; Son, Y.-W.; Ihm, J.; Kato, H.; Wang, Z. W.; Okazaki, T.; Shinohara, H.; *et al.* Bandgap Modulation of Carbon Nanotubes by Encapsulated Metallofullerenes. *Nature* **2002,** *415*, 1005–1008.
9. Koshino, M.; Tanaka, T.; Solin, N.; Suenaga, K.; Isobe, H.; Nakamura, E. Imaging of Single Organic Molecules in Motion. *Science* **2007,** *316*, 853.
10. Guan, L.; Suenaga, K.; Shi, Z.; Gu, Z.; Iijima, S. Polymorphic Structures of Iodine and Their Phase Transition in Confined Nanospace. *Nano Lett.* **2007,** *7*, 1532–1535.
11. Kitaura, R.; Nakanishi, R.; Saito, T.; Yoshikawa, H.; Awaga, K.; Shinohara, H. High-Yield Synthesis of Ultrathin Metal Nanowires in Carbon Nanotubes. *Angew. Chem., Int. Ed.* **2009,** *48*, 8298–8302.
12. Wilson, M. The Formation of Inorganic Nanotubular Structures in Carbon Nanotubes. *Nano Lett.* **2004,** *4*, 299–302.
13. Philp, E.; Sloan, J.; Kirkland, A. I.; Meyer, R. R.; Friedrichs, S.; Hutchinson, J. L.; Green, M. L. H. An Encapsulated Helical One-Dimensional Cobalt Iodide Nanostructure. *Nat. Mater.* **2003,** *2*, 788–791.
14. Baldoni, M.; Leoni, S.; Sgamellotti, A.; Seifert, G.; Mercuri, F. Formation, Structure, and Polymorphism of Novel Lowest-Dimensional AgI Nanoaggregates by Encapsulation in Carbon Nanotubes. *Small* **2007,** *3*, 1730–1734.
15. Britz, D. A.; Khlobystov, A. N. Noncovalent Interactions of Molecules with Single Walled Carbon Nanotubes. *Chem. Soc. Rev.* **2006,** *35*, 637–659.

16. Garcia-Suarez, V. M.; Ferrer, J.; Lambert, C. J. Strongly Correlated Electron Physics in Nanotube-Encapsulated Metallocene Chains. *Phys. Rev. B* **2006,** *74*, 205421.
17. Tournus, F.; Latil, S.; Heggie, M. I.; Charlier, J.-C. π-Stacking Interaction between Carbon Nanotubes and Organic Molecules. *Phys. Rev. B* **2005,** *72*, 075431.
18. Tison, Y.; Giusca, C. E.; Sloan, J.; Silva, S. R. P. Registry-Induced Electronic Superstructure in Double-Walled Carbon Nanotubes, Associated with the Interaction between Two Graphene-like Monolayers. *ACS Nano* **2008,** *2*, 2113–2120 and references therein..
19. Bendall, J. S.; Ilie, A.; Welland, M. E.; Sloan, J.; Green, M. L. H. Thermal Stability and Reactivity of Metal Halide Filled Single-Walled Carbon Nanotubes. *J. Phys. Chem. B* **2006,** *110*, 6569–6573.
20. West, A. R. *Basic Solid State Chemistry*, 2nd ed.; John Wiley & Sons Ltd.: New York, 2004.
21. Makiura, R.; Yonemura, T.; Yamada, T.; Yamauchi, M.; Ikeda, R.; Kitagawa, H.; Kato, K.; Takata, M. Size-Controlled Stabilization of the Superionic Phase to Room Temperature in Polymer-Coated AgI Nanoparticles. *Nat. Mater.* **2009,** *9*, 476–480.
22. Ilie, A.; Bendall, J. S.; Kubo, O.; Sloan, J.; Green, M. L. H. Force and Energy Dissipation Variations in Noncontact Atomic Force Spectroscopy of Composite Carbon Nanotube Systems. *Phys. Rev. B* **2006,** *74*, 235418.
23. Czerw, R.; Liu, J.; Carroll, D. L. Electronic Effects in Scanning Tunnelling Microscopy of Metal-Filled Multiwalled Carbon Nanotubes. *New J. Phys.* **2004,** *6*, 31 and references therein..
24. Ashino, M.; Obergfell, D.; Haluska, M.; Yang, S.; Khlobystov, A. N.; Roth, S.; Wiesendanger, R. Atomically Resolved Mechanical Response of Individual Metallofullerene Molecules Confined inside Carbon Nanotubes. *Nat. Nanotechnol.* **2008,** *3*, 337–341.
25. Lauffer, P.; Jung, A.; Graupner, R.; Hirsch, A.; Ley, L. Functionalization of Single-Walled Carbon Nanotubes by Aromatic Molecules Studied by Scanning Tunneling Microscopy. *Phys. Status Solidi B* **2006,** *243*, 3213–3216.
26. Czerw, R.; Guo, Z.; Ajayan, P. M.; Sun, Y.-P.; Carroll, D. L. Organization of Polymers onto Carbon Nanotubes: A Route to Nanoscale Assembly. *Nano Lett.* **2001,** *1*, 423–427.
27. Yarotski, D. A.; Kilina, S. V.; Talin, A. A.; Tretiak, S.; Prezhdo, O. V.; Balatsky, A. V.; Taylor, A. J. Scanning Tunneling Microscopy of DNA-Wrapped Carbon Nanotubes. *Nano Lett.* **2009,** *9*, 12–17.
28. Sloan, J.; Kirkland, A. I.; Hutchison, J. L.; Green, M. L. H. Integral Atomic Layer Architectures of 1D Crystals Inserted into Single Walled Carbon Nanotubes. *Chem. Commun.* **2002,** 1319–1332.
29. Eliseev, A. A.; Yashina, L. V.; Brzhezinskaya, M. M.; Chernysheva, M. V.; Kharlamova, M. V.; Verbitsky, N. I.; Lukashin, A. V.; Kiselev, N. A.; Kumskov, A. S.; Zakalyuhin, R. M.; *et al.* Structure and Electronic Properties of AgX (X = Cl, Br, I)-Intercalated Single-Walled Carbon Nanotubes. *Carbon* **2010,** *48*, 2708–2721.
30. Kiselev, N. A.; Zakalyukin, R. M.; Zhigalina, O. M.; Grobert, N.; Kumskov, A. S.; Grigoriev, Y. V.; Chernysheva, M. V.; Eliseev, A. A.; Krestinin, A. V.; Tretyakov, Y. D.; *et al.* The Structure of 1D CuI Crystals inside SWNTs. *J. Microsc.* **2008,** *232*, 335–342.
31. Chen, C. J. *Introduction to Scanning Tunneling Microscopy*, 2nd ed.; Oxford University Press Inc.: New York, 2008.
32. Ouyang, M.; Huang, J.-L.; Lieber, C. M. One-Dimensional Energy Dispersion of Single-Walled Carbon Nanotubes by Resonant Electron Scattering. *Phys. Rev. Lett.* **2002,** *88*, 066804.
33. Clauss, W.; Bergeron, D. J.; Freitag, M.; Kane., C. L.; Mele, E. J.; Johnson, A. T. Electron Backscattering on Single-Wall Carbon Nanotubes Observed by Scanning Tunneling Microscopy. *Europhys. Lett.* **1999,** *47*, 601–607.
34. Venema, L. C.; Wildoer, J. W. G.; Janssen, J. W.; Tans, S. J.; Hinne, L. J.; Tuinstra, T.; Kouwenhoven, L. P.; Dekker, C. Imaging Electron Wave Functions of Quantized Energy Levels in Carbon Nanotubes. *Science* **1999,** *283*, 52–55.
35. Hassanien, A.; Tokumoto, M.; Shimizu, T.; Tokumoto, H. STM on Suspended Single Wall Carbon Nanotubes. *Thin Solid Films* **2004,** *464−465*, 338–341.
36. Kane, C. L.; Mele, E. J. Broken Symmetries in Scanning Tunneling Images of Carbon Nanotubes. *Phys. Rev. B* **1999,** *59*, R12759–R12762.
37. Buchs, G.; Ruffieux, P.; Groning, P.; Groning, O. Scanning Tunneling Microscopy Investigations of Hydrogen Plasma-Induced Electron Scattering Centers on Single-Walled Carbon Nanotubes. *Appl. Phys. Lett.* **2007,** *90*, 013104.
38. Mizes, H. A.; Foster, J. S. Long-Range Electronic Perturbations Caused by Defects Using Scanning Tunneling Microscopy. *Science* **1989,** *244*, 559–562.
39. Osváth, Z.; Vértesy, G.; Tapasztó, L.; Wéber, F.; Horváth, Z. E.; Gyulai, J.; Biró, L. P. Atomically Resolved STM Images of Carbon Nanotube Defects Produced by Ar^+ Irradiation. *Phys. Rev. B* **2005,** *72*, 045429.
40. Kane, C. L.; Mele, E. J. Size, Shape, and Low Energy Electronic Structure of Carbon Nanotubes. *Phys. Rev. Lett.* **1997,** *78*, 1932.
41. Tekleab, D.; Carroll, D. L.; Samsonidze, G. G.; Yakobson, B. I. Strain-Induced Electronic Property Heterogeneity of a Carbon Nanotube. *Phys. Rev. B* **2001,** *64*, 035419.
42. Venema, L. C.; Meunier, V.; Lambin, P.; Dekker, C. Atomic Structure of Carbon Nanotubes from Scanning Tunneling Microscopy. *Phys. Rev. B* **2000,** *61*, 2991–2996.
43. Akai, Y.; Saito, S. Electronic Structure, Energetics and Geometric Structure of Carbon Nanotubes: A Density-Functional Study. *Physica E* **2005,** *29*, 555–559.
44. Meunier, V.; Lambin, P. Scanning Tunnelling Microscopy of Carbon Nanotubes. *Philos. Trans. R. Soc., A* **2004,** *362*, 2187–2203.
45. Lin, H.; Lagoute, J.; Chacon, C.; Girard, Y.; Ducastelle, F.; Amara, H.; Loiseau, A.; Hermet, P.; Henrard, L.; Rousset, S. Imaging the Symmetry Breaking of Molecular Orbitals in Single-Walled Carbon Nanotubes. *Phys. Rev. B* **2010,** *81*, 235412.
46. McEuen, P. L.; Bockrath, M.; Cobden, D. H.; Yoon, Y.-G.; Louie, S. G. Disorder, Pseudospins, and Backscattering in Carbon Nanotubes. *Phys. Rev. Lett.* **1999,** *83*, 5098–5101.
47. Langlet, R.; Devel, M.; Lambin, P. Computation of the Static Polarizabilities of Multi-Wall Carbon Nanotubes and Fullerites Using a Gaussian Regularized Point Dipole Interaction Model. *Carbon* **2006,** *44*, 2883–2895 and references therein..
48. The potential modulation decreases with increasing radial distance away from the nanotube's surface (not shown) so that at a typical tip−surface distance of 0.2−0.3 nm its direct contribution to the topography during constant current imaging is negligible.
49. Quantum number q (from quantization along the circumference) indexes the SWCNT's bands, while k denotes the component of $\vec{k}$ along the tube's axis, which is continuous.
50. Michalski, P. J.; Mele, E. J. Carbon Nanotubes in Helically Modulated Potentials. *Phys. Rev. B* **2008,** *77*, 085429.
51. *CrystalMaker 2.0*, CrystalMaker Software 2006.
52. Kilaas, R. 45th Ann. Proc. EMSA 1987, 66.
53. Horcas, I.; Fernandez, R.; Gomez-Rodriguez, J. M.; Colchero, J.; Gomez-Herrero, J.; Baro, A. M. WSXM: A Software for Scanning Probe Microscopy and a Tool for Nanotechnology. *Rev. Sci. Instrum.* **2007,** *78*, 013705.
54. Stroscio, J. A.; Feenstra, R. M.; Fein, A. P. Electronic-Structure of the Si(111)2 $\times$ 1 Surface by Scanning-Tunneling Microscopy. *Phys. Rev. Lett.* **1986,** *57*, 2579–2582.
55. Dovesi, R.; Saunders, V. R.; Roetti, C.; Orlando, R.; Zicovich-Wilson, C. M.; Pascale, F.; Civalleri, B.; Doll, K.; Harrison, N. M.; Bush, I. J.; *et al. CRYSTAL06 User's Manual*; University of Torino: Torino, Italy, 2006.
56. Catti, M. First-Principles Landau Potential for the Rocksalt to KOH to TlI-Type Phase Transitions of AgI. *Phys. Rev. B* **2006,** *74*, 174105.
57. Catti M. Private communication.